

Effect of three-body elastic scattering on heavy quark momentum degradation in the quark-gluon plasma

W. Liu¹ and C. M. Ko¹

¹*Cyclotron Institute and Physics Department, Texas A&M University, College Station, Texas 77843-3366*

Heavy quark drag coefficients in the quark-gluon plasma are evaluated in the perturbative QCD. It is found that for charm quarks the contribution from three-body elastic scattering is comparable to those from two-body elastic and radiative scatterings while for bottom quarks it becomes dominant. Using a schematic expanding fireball model, effects of both two-body and three-body scatterings on the transverse momentum spectra of heavy quarks produced in Au+Au collisions at center of mass energy $\sqrt{s_{NN}} = 200$ GeV are studied. Results on electrons from resulting heavy meson decays are compared with available experimental data.

PACS numbers: 12.38.Mh;24.85.+p;25.75.-q

One of the most interesting observations in central heavy ion collisions at the Relativistic Heavy Ion Collider (RHIC) is the suppressed production of hadrons with large transverse momentum (p_T) [1, 2]. This phenomenon has been attributed to the radiative energy loss of partonic jets produced from initial hard scattering of incoming nucleons as they pass through the created dense partonic matter [3, 4, 5]. The same mechanism fails, however, to explain a similarly large suppression of high p_T charmed mesons observed through their decay electrons as a result of the dead cone effect associated with massive quarks [6, 7]. Furthermore, experimental data have indicated that charm quarks develop a substantial elliptic flow in non-central heavy ion collisions at RHIC [8], consistent with the prediction of the quark coalescence model that assumes a thermally equilibrated charm quark distribution in the quark-gluon plasma (QGP) [9]. In both the Fokker-Planck approach [10] and the transport model [11, 12], to reproduce the observed strong suppression of charm production at high p_T and large charm elliptic flow requires a much larger charm quark two-body elastic scattering cross section than that given by the perturbative QCD. Such a large cross section would result if colorless resonances are formed in charm quark scattering with light quark [13]. On the other hand, it was recently realized [14] that two-body elastic scattering with the pQCD cross section causes a similar energy loss for the charm quark as the two-body radiative scattering [15], and a large fraction of the observed suppression of charmed meson production at high p_T can be accounted for when both effects are included.

Since the density of the partonic matter formed in heavy ion collisions at RHIC is large, ranging from about 1 fm^{-3} near hadronization to more than 10 fm^{-3} during the initial stage, three-body elastic scattering may also contribute to charm quark energy loss in the QGP. Previous studies have shown that gluon [16] and quark [17] three-body elastic scatterings are more efficient than two-body elastic scattering for the thermalization of initially produced partons. In the present paper, the effect of three-body elastic scattering on heavy quark ($Q = c, b$) momentum degradation in the QGP is studied.

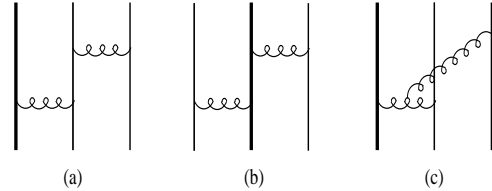


FIG. 1: Topologically different diagrams for heavy quark (thick line) three-body elastic scatterings by quarks and antiquarks (thin line) with different flavors. Wiggly lines denote the gluon.

For the processes $Qqq \rightarrow Qqq$, $Q\bar{q}\bar{q} \rightarrow Q\bar{q}\bar{q}$, and $Qq\bar{q} \rightarrow Qq\bar{q}$ with different light quark (q) and antiquark (\bar{q}) flavors, there are three topologically different diagrams in the lowest-order QCD as shown in Fig. 1. While diagram (c) corresponds to one diagram, two diagrams are generated from diagram (b), corresponding to either the left or the right gluon (wiggly line) is first exchanged, and four diagrams are generated from diagram (a) by exchanging the two gluons in all possible ways but keeping only one attached to the heavy quark.

To ensure true three-body scattering, the intermediate quark in both diagrams (a) and (b) of Fig. 1 must be off-shell, and this can be achieved by including its collisional width in the QGP and keeping only the real part of its propagator in evaluating these diagrams as in the treatment of three-body scattering in hadronic matter [18]. The quark width in QGP is given by $\Gamma/\hbar = \sum_i \langle |\mathcal{M}_i|^2 \rangle$, where the sum is over all scattering processes with $|\mathcal{M}_i|^2$ being their squared amplitudes after averaging over the spins and colors of initial partons and summing over those of final partons. The symbol $\langle \dots \rangle$ denotes average over the thermal distributions of scattered quarks and antiquarks in the QGP and integration over the momenta of all final-state partons.

We first consider the quark width due to two-body elastic and radiative scatterings as well as the inverse process of the latter. For heavy quark two-body elastic scattering, there is only one t -channel gluon-exchange diagram for the process $Qq \rightarrow Qq$ or $Q\bar{q} \rightarrow Q\bar{q}$, while there are

in addition one s -channel heavy quark pole and one u -channel heavy quark exchange diagram for the process $Qg \rightarrow Qg$. Diagrams for heavy quark two-body radiative scattering are then obtained by adding an external gluon to above diagrams, leading to 5 diagrams for the process $Qq \rightarrow Qqg$ or $Q\bar{q} \rightarrow Q\bar{q}g$ and 16 diagrams for the process $Qg \rightarrow Qgg$. For the light quark, there are additional diagrams besides those similar to the ones for heavy quarks, and all these diagrams are included in our calculations. In evaluating these diagrams, we remove the collinear singularity in t -channel diagrams by using the screening mass $m_D = gT$ [19] for the exchanged gluon, where g is the QCD coupling constant and T is the temperature of the QGP, and the infrared singularity in two-body radiative scattering by including the thermal mass $m_g = m_D/\sqrt{2}$ [19] for the radiated gluon.

Using the QCD coupling $\alpha_s = g^2/4\pi = 0.3$, appropriate for the energy scales considered here, and also including the thermal mass for time-like gluons as well as the thermal mass $m_q = m_D/\sqrt{6}$ [19] for time-like light quarks, we find that both heavy and light quark collisional widths in the QGP increase almost linearly with quark momentum as well as the temperature of the QGP. For a momentum of 4 GeV/ c , the widths are about 75 MeV for charm quark and 49 MeV for bottom quark at $T = 175$ MeV and increase, respectively, to about 130 MeV and 93 MeV at $T = 350$ MeV. These widths are mainly due to two-body elastic scattering with only about 25% from two-body radiative scattering and its inverse process. For the light quark, its width is about 50% larger than that of charm quark. Using above calculated quark widths in the quark propagator, we find that three-body elastic scattering by quarks and antiquarks with different flavors increases quark widths by at most 10% and can thus be neglected. We note that since the heavy quark width is smaller than the gluon thermal mass ($\Gamma_Q < m_g$), i.e., the time between heavy quark collisions is longer than the time for radiating a thermal gluon, the destructive Landau-Pomeranchuk-Migdal (LPM) interference effect [20], which is neglected in present study, is expected to be small for heavy quark two-body radiative scattering as shown in Ref.[20].

In the Fokker-Planck approach, the momentum degradation of a heavy quark in the QGP depends on its drag coefficient, which is given by averages similar to that for the quark collisional width, i.e., $\gamma(|\mathbf{p}|, T) = \langle |\overline{M}|^2 \rangle - \langle |\overline{M}|^2 \mathbf{p} \cdot \mathbf{p}' \rangle / |\mathbf{p}|^2$ [13, 21]. In the above, \mathbf{p} and \mathbf{p}' are, respectively, the momenta of the heavy quark before and after a collision. In Fig. 2, we show the charm (upper panels) and bottom (lower panels) quark drag coefficients as functions of their momentum in QGP at temperatures $T = 200$ MeV (left panels) and $T = 300$ MeV (right panels). It is seen that for charm quarks the contribution from three-body scattering by light quarks and antiquarks with different flavors (dash-dotted line) is generally smaller than those from two-body elastic (dotted line) and radiative scatterings (dashed line). For bottom quarks, the most important contribution is from

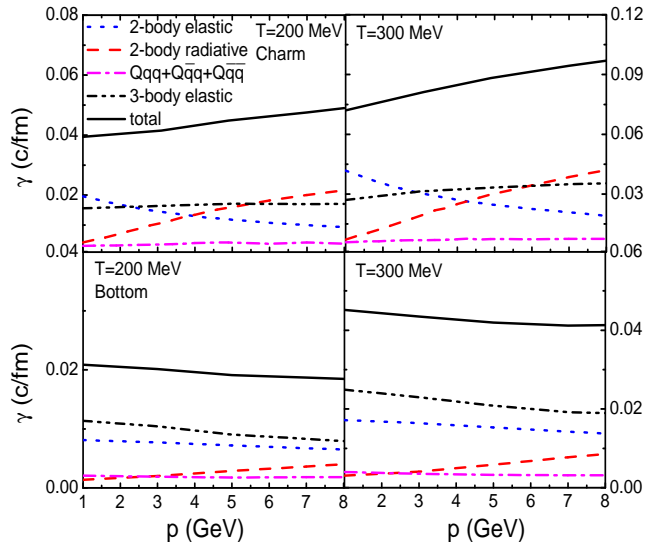


FIG. 2: Charm (upper panels) and bottom (lower panels) quark drag coefficients as functions of their momentum in a QGP of temperature $T = 200$ MeV (left panels) or $T = 300$ MeV (right panels).

two-body elastic scattering while two-body radiative and three-body elastic scattering give smaller but comparable contributions. We note that the contribution from diagram (b) of Fig. 1 is larger than that from diagram (a) by about one order of magnitude and that from diagram (c) by about two orders of magnitude.

If the two light quarks or antiquarks in Fig. 1 have same flavor, the number of diagrams is then doubled from interchanging final two light quarks or antiquarks. These exchange diagrams give same contribution as that due to the direct diagrams in Fig. 1. For the process $Qq\bar{q} \rightarrow Qq\bar{q}$ with same quark and antiquark flavor, besides diagrams similar to those of Fig. 1, the quark and antiquark can annihilate to a time-like virtual gluon, giving rise to additional five diagrams corresponding to different ways a gluon is exchanged between the heavy quark and the light quark, antiquark, and time-like gluon. The contribution from these annihilation diagrams is found to be small, and this allows us to neglect the interference between these diagrams and the diagrams in Fig. 1. Neglecting also the small interference terms between above direct and exchange diagrams for scattering by two identical quarks or antiquarks, the contribution from quarks and antiquarks with same flavor is then the same as that from quarks and antiquarks with different flavors.

For heavy quark three-body elastic scattering involving gluons, there are 36 diagrams for the process $Qqg \rightarrow Qqg$ or $Q\bar{q}g \rightarrow Q\bar{q}g$, and 123 diagrams for the process $Qgg \rightarrow Qgg$. We have not been able to evaluate all these diagrams. Instead, we assume that these processes are also dominated by diagrams similar to diagram (b) of Fig. 1. This is also partially supported by the finding

that for the process $qgg \rightarrow qgg$ involving a light quark the result obtained from including thermal and screening masses in the Parke formula [22] that takes into account many diagrams with topologies different from that of diagram (b) of Fig. 1 indeed gives a much smaller contribution to the quark drag coefficient. Within this approximation, the contribution from $Qgg \rightarrow Qgg$ to heavy quark drag coefficients is slightly smaller while that from $Qqg \rightarrow Qqg$ and $Q\bar{q}g \rightarrow Q\bar{q}g$ is about a factor of three larger than that due to scattering by quarks and antiquarks, essentially due to the associated color and flavor factors in these processes. Because of the importance of $Qqg \rightarrow Qqg$ and $Q\bar{q}g \rightarrow Q\bar{q}g$, the heavy quark width is significantly increased by three-body elastic scattering. Including this additional width in the intermediate heavy quark propagator in diagram (b) of Fig. 1 leads to a charm quark drag coefficient due to three-body elastic scattering (dash-dot-dotted line in Fig. 2) that is comparable to that due to two-body elastic or radiative scattering, and a bottom quark drag coefficient that is now dominated by three-body elastic scattering. The resulting total drag coefficients for heavy quarks due to both elastic two- and three-body scattering are shown by solid lines in Fig. 2.

To see the effect of three-body elastic scattering on heavy quark momentum degradation in QGP, we consider central Au+Au collisions at center-of-mass energy $\sqrt{s_{NN}} = 200$ GeV. The initial p_T spectra of charm and bottom quarks at midrapidity are taken to be $dN_c/d^2p_T = 19.2[1 + (p_T/6)^2]/\{(1 + p_T/3.7)^{12}[1 + \exp(0.9 - 2p_T)]\}$ and $dN_b/d^2p_T = 0.0025 [1 + (p_T/16)^5] \exp(-p_T/1.495)$, respectively, with p_T in unit of GeV/c. Both are obtained by multiplying the heavy quark p_T spectra from p+p collisions at same energy by the number of binary collisions (~ 960) in Au+Au collisions. For bottom quarks, their p_T spectrum in p+p collisions is taken from the pQCD prediction of Ref.[23] as it is expected to be more reliable, while for charm quarks it is determined instead from fitting simultaneously measured p_T spectrum of charmed mesons from d+Au collisions [24] and of electrons from heavy meson decays in p+p collisions. In obtaining the latter, heavy quarks are fragmented to hadrons via the Peterson fragmentation function $D(z) = 1/\{z[1-1/z-\epsilon/(1-z)]^2\}$ [25], where z is the fraction of heavy quark momentum carried by the formed meson, with ϵ taken to be 0.02 for charm quarks and 0.002 for bottom quarks in order to reproduce the empirical fragmentation functions used in Ref.[23]. These heavy quarks are initially distributed in the transverse plane according to that of the binary collision number, and their transverse momenta are directed isotropically in the transverse plane.

For the dynamics of formed QGP, we assume that it evolves boost invariantly in the longitudinal direction but with an accelerated transverse expansion. Specifically, its volume expands in the proper time τ according to $V(\tau) = \pi R(\tau)^2 \tau$, where $R(\tau) = R_0 + a/2(\tau - \tau_0)$ is the transverse radius with an initial value $R_0=7$ fm, $\tau_0=0.6$

fm is the QGP formation time, and $a = 0.1c^2/\text{fm}$ is the transverse acceleration [26]. With an initial temperature $T_i = 350$ MeV and using thermal masses for quarks and gluons, this model gives a total transverse energy comparable to that measured in experiments. The time dependence of the temperature is then obtained from entropy conservation, and the critical temperature $T_c = 175$ MeV is reached at proper time $\tau_c \sim 5$ fm.

For a heavy quark with an initial transverse momentum \mathbf{p}_0 , time evolution of its mean transverse momentum $\langle p_T \rangle$ can be obtained from the Fokker-Planck equation, i.e., $d\langle p_T \rangle/dt = -\langle \gamma(p_T, T) p_T \rangle$. Parametrizing the momentum dependence of heavy quark drag coefficients shown in Fig. 2 by $\gamma(p_T, T) \approx \gamma_0(T)[1 + ap_T]$, we then have $d\langle p_T \rangle/dt \approx -\gamma_0(\langle p_T \rangle + a\langle p_T^2 \rangle) \approx -\gamma_0(\langle p_T \rangle + a\langle p_T \rangle^2)$ if we take $\langle p_T^2 \rangle \approx \langle p_T \rangle^2$, which is valid for high transverse momentum heavy quarks as considered here. The final mean transverse momentum of the heavy quark after passing through the expanding QGP is then given by $\langle p_T \rangle = B/(1 - aB)$, where $B = p_0 \exp(-\int_{\tau_0}^{\tau_f} \gamma_0(\tau) d\tau)/(1 + ap_0)$ with τ_f denoting the smaller of the time when the QGP phase ends and the time for the heavy quark to escape the expanding QGP, which depends on its initial transverse momentum and position. The final p_T spectra of heavy quarks are then obtained by averaging over their initial spatial and transverse momentum distributions.

Besides fragmenting to mesons, heavy quarks produced in heavy ion collisions can also coalesce or recombine with thermal quarks in the QGP to form heavy mesons [9, 12]. In both hadronization mechanisms, the momentum spectra of formed mesons are softer than those of heavy quarks. Instead of including both contributions, we use the fragmentation model in the present study for simplicity. Because of their smaller scattering cross sections with hadrons [27] and lower hadronic matter density, momentum degradation of heavy mesons in subsequent hadronic matter is small [12] and is thus neglected. The heavy mesons produced from heavy quark fragmentation are therefore allowed to decay directly to electrons in order to compare with those measured in experiments.

In the left panel of Fig. 3, we show our results for the initial (dash-dot-dotted lines) and final p_T spectra of heavy quarks in Au+Au collisions at $\sqrt{s_{NN}} = 200$ GeV. For both charm and bottom quarks, their final p_T spectra become softer with the inclusion of more scattering processes: dotted lines for two-body elastic scattering only, dashed lines for both two-body elastic and radiative scatterings, dash-dotted lines for adding also three-body scattering by light quarks and antiquarks with different flavors, and solid lines for further including other three-body scattering processes. Although bottom quarks are negligible at low transverse momentum, they are important at high transverse momentum as a result of their smaller momentum degradation in QGP than charm quarks. Due to larger bottom quark mass, electrons from their decays become dominant at high p_T as shown in the middle panel of Fig. 3. The ratio of the electron p_T spec-

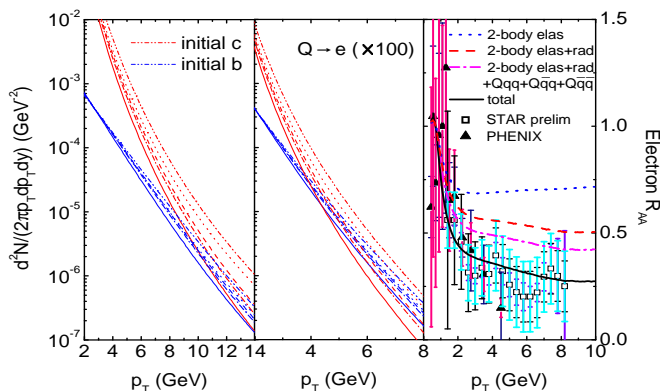


FIG. 3: Initial and final transverse momentum spectra of heavy quarks (left panel) and their decay electrons (middle panel) as well as the nuclear modification factor R_{AA} for electrons (right panel) in central Au+Au collisions at $\sqrt{s_{NN}} = 200$ GeV.

trum from final heavy mesons to that from initially produced ones, defined as the electron nuclear modification factor R_{AA} , is shown in the right panel of Fig. 3. It is seen that the effect from two-body elastic scattering (dotted line) is as important as that from two-body radiative scattering, similar to that of Ref.[14]. The electron R_{AA} including both contributions (dashed line) is, however, slightly above the experimental data from the PHENIX collaboration (filled triangles) [28] and the preliminary data from the STAR collaboration (open squares) [29]. Adding the contribution from charm quark three-body elastic scattering leads to an electron R_{AA} that is in rea-

sonable agreement with the measured one as shown by the solid line. If we include only charm quark three-body scattering by light quarks and antiquarks of different flavors, which is more reliably computed in present study, the resulting electron R_{AA} is shown by the dash-dotted line which barely lies on the upper error bars of experimental data.

Our results indicate that heavy quark three-body elastic scattering is important for understanding the electron nuclear modification factor in heavy ion collisions at RHIC. The most important heavy quark three-body elastic scattering process involves scattering with a gluon and a light quark or antiquark in the QGP, and this contribution has been evaluated using the assumption that they are dominated by t -channel gluon-exchange diagrams similar to diagram (b) of Fig. 1 for three-body scattering by quarks and antiquarks with different flavors. Although we have shown that this is a valid approximation for the latter process, its validity in heavy quark three-body elastic scattering involving gluons remains to be verified. If more accurate calculations indeed give as large a three-body contribution as shown here, then scattering involving more than three particles may also need to be considered. To evaluate the latter contribution poses, however, a major theoretical challenge.

We wish to thank Hendrik van Hees, Ralf Rapp, and Bin Zhang for helpful discussions. This work was supported in part by the US National Science Foundation under Grant No. PHY-0457265 and the Welch Foundation under Grant No. A-1358.

-
- [1] A. Adcox *et al.* [PHENIX Collaboration], Phys. Rev. Lett. **88**, 022301 (2002).
- [2] C. Adler *et al.* [STAR Collaboration], Phys. Rev. Lett. **89**, 202301 (2002); **90**, 082302 (2002).
- [3] X.N. Wang, Phys. Lett. B **579**, 299 (2004).
- [4] M. Gyulassy, P. Lévai, and I. Vitev, Phys. Rev. Lett. **85**, 5535 (2001).
- [5] U.A. Wiedemann, Nucl. Phys. B **588**, 303 (2000).
- [6] Y.L. Dokshitzer and D.E. Kharzeev, Phys. Lett. B **519**, 199 (2001).
- [7] M. Djordjevic, M. Gyulassy, and S. Wicks, Phys. Rev. Lett. **94**, 112301 (2005).
- [8] S.S. Adler *et al.* [PHENIX Collaboration], Phys. Rev. C **72**, 024901 (2005).
- [9] V. Greco, C.M. Ko, and R. Rapp, Phys. Lett. B **595**, 202 (2004).
- [10] G.D. Moore and D. Teaney, Phys. Rev. C **71**, 064904 (2005).
- [11] D. Molnar, J. Phys. G **31**, S421 (2005).
- [12] B. Zhang, L.W. Chen, and C.M. Ko, Phys. Rev. C **72**, 024906 (2005).
- [13] H. van Hees and R. Rapp, Phys. Rev. C **71**, 034907 (2005); H. van Hees *et al.*, nucl-th/0508055.
- [14] S. Wicks *et al.*, nucl-th/0512076.
- [15] M.G. Mustafa *et al.*, Phys. Lett. B **428**, 234 (1998).
- [16] X.M. Xu *et al.*, Nucl. Phys. A **744**, 347 (2004).
- [17] X.M. Xu *et al.*, Phys. Lett. B **629**, 68 (2005).
- [18] G. Batko *et al.*, Nucl. Phys. A **536**, 786 (1992).
- [19] J.P. Blaizot and E. Iancu, Phys. Rep. **359**, 355 (2002).
- [20] M. Djordjevic and M. Gyulassy, Nucl. Phys. A **733**, 265 (2004).
- [21] B. Svetitsky, Phys. Rev. D **37**, 2484 (1988).
- [22] M. Mangano and S.J. Parke, Phys. Rep. **200**, 301 (1991).
- [23] M. Cacciari *et al.*, Phys. Rev. Lett. **95**, 122001 (2005).
- [24] J. Adams *et al.* [STAR Collaboration], Phys. Rev. Lett. **94**, 062301 (2005).
- [25] R.V. Gavai *et al.*, Int. J. Mod. Phys. A **10**, 2999 (1995).
- [26] L.W. Chen *et al.*, Phys. Lett. B **601**, 34 (2004).
- [27] Z.W. Lin *et al.*, Nucl. Phys. A **689**, 965 (2001).
- [28] S.S. Adler [PHENIX Collaboration], nucl-ex/0510047.
- [29] J. Bielcik [STAR Collaboration], nucl-ex/0511005.